Experimental Signature of the Pair-Trajectories of Rough Spheres in the Shear-Induced Microstructure in Non-Colloidal Suspensions

Frédéric Blanc, François Peters, Elisabeth Lemaire

Experimental Signature of the Pair-Trajectories of Rough Spheres in the Shear-Induced Microstructure in Non-Colloidal Suspensions

Frédéric Blanc, François Peters, and Elisabeth Lemaire
CNRS, Université de Nice, LPMC-UMR 6622, 06108 Nice Cedex 2, France
(Dated: November 28, 2011)

The shear-induced microstructure in a semi-dilute non-colloidal suspension is studied. A high resolution Pair Distribution Function in the plane of shear is experimentally determined. It is shown to be anisotropic, with a depleted direction close to the velocity axis in the recession quadrant. The influence of roughness on the interaction between particles is quantitatively evidenced. The experimental results compare well with a model from particle pair trajectories.

The influence of the particle interactions on the rheology of non-Brownian suspensions, such as normal stress differences and shear-induced migration, and their link with the shear-induced microstructure, are questions of central interest and remain an experimental challenge. A quantitative measurement of the microstructure is provided by the Pair Distribution Function (PDF). Since the pioneering work of Bossis and Brady[1], in Stokesian Dynamics, the PDF of an unbounded suspension of interacting spheres undergoing a simple shear flow is known to have an angular dependence. In a semi-dilute suspension, experimental [2], numerical [3, 4] and analytical [5] studies have shown the existence of a particle depleted area along the velocity direction. In their numerical work, Drazer at al. [4] showed that, besides this anisotropy, a fore-aft asymmetry appears in the presence of strong enough non-hydrodynamic forces acting between the spheres. Repulsion forces between particles eliminate closed orbit trajectories and the particles that were close from each other in the approach quadrant are redistributed in the recession quadrant, leading downstream to a tilt of the depleted area away from the velocity direction. Though only a few experimental measurements of PDF have been performed in non-Brownian suspensions [6, 7], the depleted area close to the velocity direction in a simple shear flow has already been accurately studied by Rampall et al. in semi-dilute suspensions (ϕ=0.10-0.15). They explain their experimental results by a model that computes the PDF from the trajectories of two colliding rough spheres. Besides the depleted area, their theoretical PDF shows fore-aft asymmetry. These predictions are in qualitative agreement with their experimental results. However these early measurements suffer from a quite low resolution that precludes a fully quantitative comparison.

In this letter, we report the measurement of a high resolution PDF in a semi-dilute sheared suspension. The results are in qualitative agreement with the works mentionned above but demonstrate a new property: in the recession quadrant, right above the depleted zone, a tail-like high particle concentration zone is apparent, that is not present in the approach quadrant. A trajectory-based model shows that this tail is a direct signature of the pair-trajectories of rough spheres in the shear-induced microstructure.

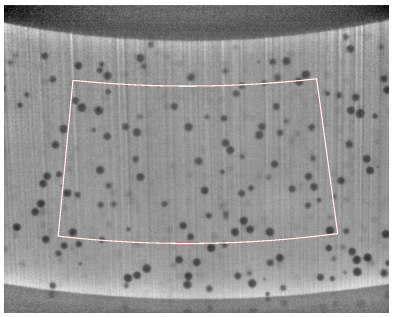

FIG. 1: Typical image. $\phi = 5\%$. Only the origin particles in the white box are considered.

This has been observed with a suspension of PMMA particles (Arkema BS510) dispersed in a Newtonian liquid (η_0= 0.85 Pa.s) designed by Cargille Laboratories (Immersion liquid Code 11295101160) in order to match both the density (d=1180kg.m^{-3}) and the refractive index (n=1.49) of the particles. To improve the index matching, the temperature is controlled (T = 37 °C). The particles are sieved to reduce the initially large size distribution. The final size distribution is determined by direct microscope observation over several hundreds of particles. The particles diameter is 2a=170 $\pm$12μm. The suspension is sheared in a cylindrical Couette cell, R_i=19mm in inner radius, R_o=24 mm in outer radius and 60 mm in height. The whole apparatus design is precisely discribed in [8, 9]. Some fluorescent dye (Nile Blue A) is dissolved in the host liquid and a thin laser sheet (635 nm, 30 μm in thickness), perpendicular to the cell axis, illuminates the suspension. The position of the laser sheet, 11 mm above the bottom of the cell, allows to neglect the bottom end effect on the flow [8]. A CCD camera positioned under the cell and equipped with a long pass filter (650nm) images the interstitial fluid, showing the particles in negative (Fig.1).

The particle positions and radii are detected using an open source Matlab procedure based on the Circular Hough Transform [10, 11]. The position of the particle

centers is determined with a subpixel resolution. For the sake of comparison, the mean particle radius a=85μm corresponds to 14.7 pixels on the frame. The inner cylinder angular velocity is controlled by a rheometer (Mars II, Thermofisher) and set to the value Ω =1 rpm. The Reynolds number $Re = (a^2 d/\eta_0)\Omega\, R_i/(\mathrm{R}_o\text{-}\mathrm{R}_i) \approx 4.10^{-6}$ and the Péclet number $Pe = (\eta_0 a^3/k_B T)\Omega R_i/(\mathrm{R}_o\text{-}\mathrm{R}_i) \approx 6.10^7$ allow to neglect inertia and Brownian motion. The shear rate $\dot{\gamma} = 2\Omega R_i^2 R_o^2/((\mathrm{R}_o^2\text{-}\mathrm{R}_i^2)\mathrm{R}^2)$ depends on the distance to the cylinders center R, and its variation across the gap is approximately 50%. This is not a problem however, since at low concentration, the non-brownian suspension rheology does not depend on the shear rate.

For each frame, a 2D PDF is built in the following way. First, for each particle pair, the relative position vector of the pair in the local flow direction frame of particle 1 is determined (see Fig.2(a)). The plane of the particles relative position $\vec{r}_{12}$ (ρ,θ) is evenly sampled ($\Delta\rho$=1 pixel, $\Delta\theta$ =2 π/80 rad), and the number of particle pairs (1,2) corresponding to a particular sample $N(\rho,\theta)$ is normalized by the total number of origin particles N_1, by the sample surface, and by the mean surface density of particles n_{0S}.

$$g(\rho,\theta) = \frac{1}{n_{0S}} \frac{N(\rho,\theta)}{N_1\, \rho\Delta\rho\Delta\theta} \qquad (1)$$

The PDF is then averaged over all images. $g(\rho,\theta)$ is thus a surface distribution function, that is related to the real 3D PDF through the integration over an interval [-2Δz_{max},2Δz_{max}] in the z direction, as explained in [2] and shown in Fig.2(b). To reduce this interval, an histogram of the apparent radii of the detected particles is built, and only particles greater than or equal to 13 pixels (0.88a) are taken into account. From this, we evaluate Δz_{max} to approximately 0.5a (Fig.2). To avoid frame boundary effects on the large ρ limit of $g(\rho,\theta)$, all origin particles (1) outside a central area are rejected (Fig.1). The distance of the box edges to the frame edges is larger than 11a. In addition, in order to reduce the hydrodynamic wall effects, no particle (2) closer than an arbitrary distance of 3a to the inner or outer cylinder is considered. Thus, the PDF should not suffer any frame boundary induced spurious decrease for interparticle distances smaller than 8a.

We turn now to the PDF measured for a ϕ = 5% suspension. 50000 frames are recorded at the rate 0.33 fps during more than 41 hours. We have checked that the PDF computed using the frames 1 to 10000 was not different from the PDF shown here, except for statistical noise, suggesting that any transient state can be neglected. Actually, we evaluate the transient time to the time necessary to break the closed orbits, i.e. the collision time $1/\dot{\gamma} \approx 3s$ that is much smaller than the experiment duration. Fig. 3 displays the measured PDF. As already shown by Rampall et al. [2], the PDF is anisotropic, with a depleted area in the approximate direction of the flow velocity. To be specific, as shown in Fig.4, the depleted direction is situated around the angle $\theta \approx 6°$in the recession quadrant. This slight tilt angle away from the velocity axis suggests some particle roughness. Away from this depleted direction, at large distance from the origin, the PDF is quite isotropic, with a value close to 1, as expected from the normalization in Eq.1. We note in passing that any strong influence of the walls or of a possible concentration gradient, that would destroy this symmetry, can be ruled out. Another classical property is the large increase of the PDF near the surface ρ=2a. Moreover, thanks to the large number of frames that leads to a high-resolution PDF, we observe for the first time a tail-like high particle concentration zone in the recession quadrant, that is not present in the approach quadrant.

This high concentration tail clearly recalls the relative trajectory of two rough particles in a simple shear flow (Fig.5). As we will show in the following, this tail allows

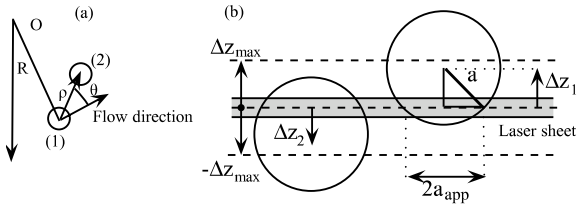

FIG. 2: (a) Pair position vector relative to the local azimuthal flow direction (b) a_{app} is the apparent radius of the particle.

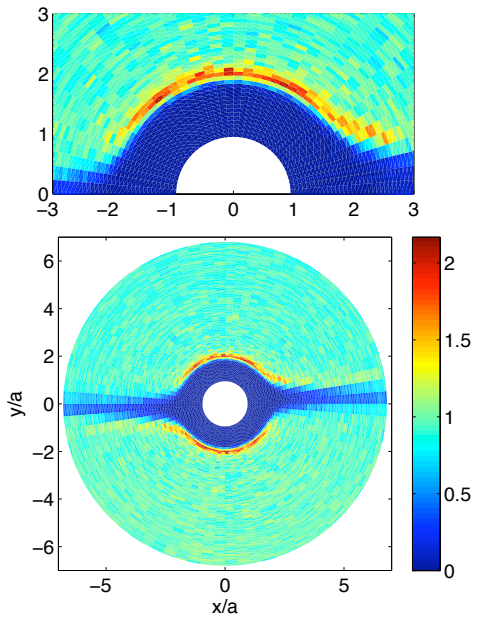

FIG. 3: Pair distribution function in the plane $(\vec{v},\vec{\nabla}v)$. ϕ =5%. The approach quadrants are defined by xy<0. Up: magnification of the central region.

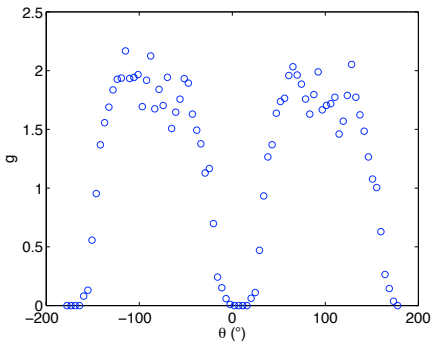

FIG. 4: PDF averaged over the ρ-interval [1.97a 2.04a]. The approach quadrant is $\theta \in [90°, 180°]$.

a good estimation of the particles roughness. Indeed, such roughness-modified trajectories have already been used to compute the shear-induced diffusivity in a dilute suspension [12]. In their paper, a roughness length ϵa is defined. When the distance between the particles equals (2+ϵ)a, the relative radial velocity is cancelled, preventing the particles to get closer from each other. This results in a break of the fore-aft symmetry, the spheres separating on streamlines further apart than on their approach (Fig.5). Following the idea of Rampall et al. [2], we use the roughness-modified trajectories to compute the PDF. For an introductory purpose, we recall here the classical isotropic expression obtained by Batchelor and Green for the PDF from the motion of two smooth particles in an ambient linear flow[13, 14].

$$g_{BG}(r) = \frac{1}{1-A(r)} exp\left(\int_r^\infty \frac{3}{s}\frac{B(s)-A(s)}{1-A(s)}ds\right) \quad (2)$$

where A and B are mobility functions that depend only on the interparticle distance r, and whose expressions can be found in [12]. Eq.(2) applies everywhere a trajectory comes from infinity. In a simple shear flow however, there exists an infinite region of closed trajectories in which it is impossible to predict the PDF values. In the plane of shear, the particles that undergo such closed orbits approach each other at a distance smaller than approximately 2.00004 a [12, 15]. Following Rampall et al. [2], and in agreement with the numerical work of Drazer et al. [3], we suppose that, owing to the roughness that prevents particles to come too close to each other, the bound pairs are eliminated. Thus, only the trajectories from infinity will be taken into account.

We use the expression of the mobility functions A(r) and B(r) given in [12] to compute the relative velocity $\vec{V}$ of two particles in a simple shear flow $\vec{V}_\infty = \dot{\gamma} y\ \vec{e}_x$, together with their relative trajectory. A(r) is set to 1 when contact occurs at r=(2+ϵ)a. The integration scheme, namely a variable order Adams-Bashforth-Moulton predictor-corrector solver, was tested as in [12] for ϵ=0 and provided the same results. Fig.5 displays trajectories in the plane of shear for different values of the roughness length. For a given value of ϵ, all trajectories that drive the particles in contact concentrate downstream on a single trajectory. Thus, downstream, no particle can locate between the x-axis and this trajectory. We note that the displacement of the trajectories depends strongly on ϵ. To determine the PDF, we compute the trajectories from evenly spaced origins in the plane (x_0=-10a), with a sample time Δt=0.01/$\dot{\gamma}$. The set of trajectories forms a distribution of particle positions $\vec{r}$ in the probability space, and each point has a velocity $\vec{V}$. Since the number of particles is conserved, this distribution is a discrete form of a function $p(\vec{r})$ that obeys Eq.3:

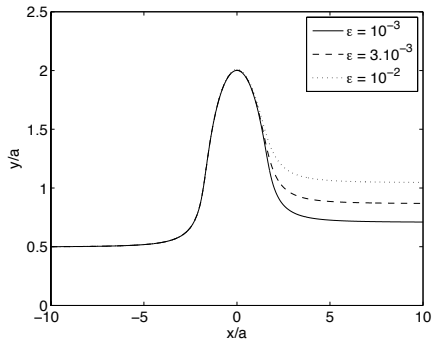

FIG. 5: Trajectory from the point x/a=-10, y/a=0.5, z/a=0 for different values of the roughness ϵa

$$\frac{\partial p}{\partial t} + \vec{\nabla}.\left(p\vec{V}\right) = \vec{\nabla}.\left(p\vec{V}\right) = 0 \quad (3)$$

We recall [3, 14] here that the PDF $g(\vec{r})$ is related to the conditional probability P($\vec{r}|\vec{r}_0$=0) of finding a sphere with its center at $\vec{r}$ given that there is a sphere with its center at $\vec{r}_0$=0 and the bulk density of particles n_0 through the equation g($\vec{r}$)=P($\vec{r}|\vec{r}_0$=0)/n_0. Since P($\vec{r}|\vec{r}_0$=0) obeys Eq.3 too [14], it is sufficient to impose the limit p$\to$1 as r$\to\infty$ to set p($\vec{r}$)=g($\vec{r}$). To this purpose, each trajectory is weighted by the inverse of the density in the plane x=x_0, namely $L_y\, L_z\, V_x(x_0)\, \Delta t$, where L_y and L_z are the distances between the trajectories origins in that plane along the directions y and z. From this set of points, we compute the relevant 2D PDF that could be compared to our experimental results. The region of interest is defined by $z \in [-2\Delta z_{max}, 2\Delta z_{max}], \rho = \sqrt{x^2+y^2} \in [2a, R_{max}]$ where we chose R_{max}=4a. This region is sampled in polar coordinates with the sampling periods $\Delta\rho$=a/15, $\Delta\theta$=π/40, and the number of points in each cell divided by its volume $4\Delta z_{max}\, \Delta(\rho^2)/2\, \Delta\theta$ gives the sought PDF.

We restrict the plane (x=x_0=-10a) of trajectory origins outside the closed orbits region. In order the PDF to be smooth enough, the value of the sampling period in

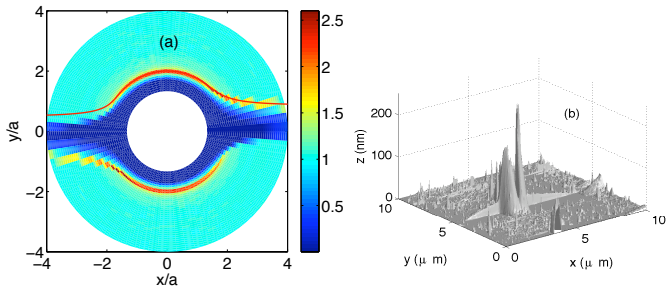

FIG. 6: (a) PDF from particle trajectories. The roughness is ϵ=3.10^{-3}. Red line: a trajectory in the plane of shear for which contact occurs. (b) AFM image of the particle surface.

the plane $x = x_0$ have been chosen: $L_z/(2\Delta z_{max})$=1/20, L_y/a=1/50. Δz_{max}=0.5a has been manually adjusted to fit the experimental data at best. We note that this value corresponds also to the estimation of Δz_{max} from the distribution of particle radii (Fig.2(b)). We have checked that this method yield the isotropic distribution of Eq.2 in the case of a pure strain flow. Concerning the simple shear flow, we obtain the PDF in Fig.6.a for a roughness ϵa=3.10^{-3}a=255nm. A trajectory in the plane of shear for which contact occurs is also shown for the same roughness. It is centered on the tail in the recession quadrant. We have checked that away from the depleted area and the tail, the PDF is identical to the isotropic g_{BG} of Eq.2, in agreement with [3]. Fig.7.a displays the experimental and computed PDF g(ρ,θ) as a function of θ for two values of the distance ρ. The agreement is very good, especially concerning the position of the tail that appears clearly on the experimental curve. The radial profiles can be compared on Fig.7.b for three different angles. The model describes accurately the experimental PDF, both in the direction of the velocity gradient (85.5° < θ <90°) and near the depleted direction (18° < θ <22.5°). However, in the depleted direction (0° < θ <4.5°), the model predicts the total lack of particles in contrast to the experimental results. As already mentioned in [2], this is probably the consequence of multibody effects. Finally, we have performed surface roughness measurements on the particles using an Atomic Force Microscope. The main roughness height is small (≈20nm), with isolated bumps, approximately 200 nm in height, as shown on Fig.6.b. Those bumps are frequent, even if we did not perform any extensive statistical study. These direct measurements are fully consistent with the experimental PDF.

In conclusion, we have measured a high resolution PDF in a sheared dilute suspension. Its fore-aft asymmetry is quantitatively explained by the particle roughness as modeled by a minimum approach distance between particles ϵa [12], which can be determined with reasonable accuracy. Some experiments are currently performed on

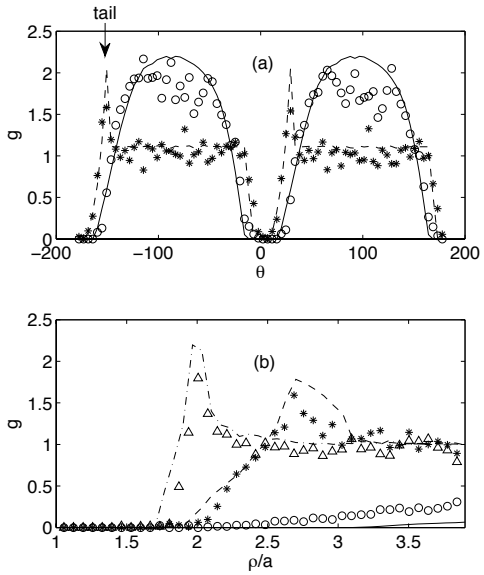

FIG. 7: Experimental (symbols) and computed (lines) PDF. **(a)** g(ρ,θ) vs θ (∘) 1.97 < ρ < 2.04; (∗) 2.31 < ρ < 2.38; (–) 1.93 < ρ < 2.00; (– –) 2.33 < ρ < 2.40; **(b)** g(ρ,θ) vs ρ/a (∘) 0 < θ < 4.5; °(∗) 18°< θ < 22.5 °; (△) 85.5°< θ < 90; °; (–) 0 < θ < 4.5°; (– –) 18°< θ < 22.5°; (– ·) 85.5°< θ < 90°

more concentrated suspensions (ϕ=0.10-0.55). In the semi-dilute regime, we observe that the tilt angle from the velocity axis hardly depends on the volume fraction. For volume fractions higher than 0.2, the tilt angle increases with the particle concentration, as already reported by Drazer et al.[3]. In addition, the tail turns blurred, partly due to poorer statistics (1000 frames per PDF), but also to increasingly large multibody effects, that modify the pair trajectories.

We are grateful to L. Lobry for fruitful discussions, and A. Zenerino for the AFM images. This work was supported by the ANR (Program No. ANR-08-BLAN-0048-CSD 2).

[1] G. Bossis and J. Brady, J. Chem. Phys. **80**, 5141 (1984).
[2] I. Rampall, J. Smart, and D. Leighton, J. Fluid Mech. **339**, 1 (1997).
[3] G. Drazer, J. Koplik, B. Khusid, and A. Acrivos, J. Fluid Mech. **511**, 237 (2004).
[4] G. Drazer, J. Koplik, B. Khusid, and A. Acrivos, Journal of Fluid Mechanics **460**, 307 (2002).
[5] H. Wilson and R. Davis, Journal of Fluid Mechanics **421**, 339 (2000).
[6] D. Husband and F. Gadala-Maria, J. Rheol. **31**, 95 (1987).
[7] F. Parsi and F. Gadala-Maria, J. Rheol. **31**, 725 (1987).
[8] F. Blanc, F. Peters, and E. Lemaire, Appl. Rheol. **11**, 23735 (2011).
[9] F. Blanc, F. Peters, and E. Lemaire, J. Rheol. **55**, 835

(2011).
[10] T. Peng, http://www.mathworks.com/matlabcentral/fileexchange/9168.
[11] C. Kimme, D. Ballard, and J. Sklansky, Commun. ACM **18**, 120 (1975).
[12] F. Da Cunha and E. Hinch, J. Fluid Mech. **309**, 211 (1996).
[13] G. Batchelor and J. Green, J. Fluid Mech. **56**, 375 (1972).
[14] G. K. Batchelor and J. T. Green, J. Fluid Mech. **56**, 401 (1972).
[15] P. Arp and S. Mason, J. Colloid Interf. Sci. **61**, 21 (1977).